Journal of Inorganic Biochemistry 262 (2025) 112763

Contents lists available at ScienceDirect

Journal of Inorganic Biochemistry

journal homepage: www.elsevier.com/locate/jinorgbio

Catalytic and post-translational maturation roles of a conserved active site serine residue in nitrile hydratases

Callie Miller [a], Kylie Knutson [a], Dali Liu [b], Brian Bennett [c], Richard C. Holz [a,*]

[a] Department of Chemistry, Colorado School of Mines, Golden, CO 80401, USA
[b] Department of Chemistry and Biochemistry, Loyola University, Chicago, IL 60660, USA
[c] Department of Physics, Marquette University, 540 N. 15th St, Milwaukee, WI 53233, USA

ARTICLE INFO

Keywords:
Nitrile hydratase
Cobalt
Metallochaperone
Mutagenesis
Serine

ABSTRACT

A highly conserved second-sphere active site αSer residue in nitrile hydratase (NHase), that forms a hydrogen bond with the axial metal-bound water molecule, was mutated to Ala, Asp, and Thr, in the Co-type NHase from *Pseudonocardia thermophila* JCM 3095 (*Pt*NHase) and to Ala and Thr in the Fe-type NHase from *Rhodococcus equi* TG328–2 (*Re*NHase). All five mutants were successfully purified; metal analysis via ICP-AES indicated that all three Co-type *Pt*NHase mutants were in their apo-form while the Fe-type αSer117Ala and αSer117Thr mutants contained 85 and 50 % of their active site Fe(III) ions, respectively. The k_{cat} values obtained for the *Pt*NHase mutant enzymes were between 0.03 ± 0.01 and 0.2 ± 0.02 s^{-1} amounting to <0.8 % of the k_{cat} value observed for WT *Pt*NHase. The Fe-type *Re*NHase mutants retained some detectable activity with k_{cat} values of 93 ± 3 and 40 ± 2 s^{-1} for the αSer117Ala and αSer117Thr mutants, respectively, which is ~5 % of WT *Re*NHase activity towards acrylonitrile. UV–Vis spectra coupled with EPR data obtained on the *Re*NHase mutant enzymes showed subtle changes in the electronic environment around the active site Fe(III) ions, consistent with altering the hydrogen bonding interaction with the axial water ligand. X-ray crystal structures of the three *Pt*NHase mutant enzymes confirmed the mutation and the lack of active site metal, while also providing insight into the active site hydrogen bonding network. Taken together, these data confirm that the conserved active site αSer residue plays an important catalytic role but is not essential for catalysis. They also confirm the necessity of the conserved second-sphere αSer residue for the metalation process and subsequent post-translational modification of the α-subunit in Co-type NHases but not Fe-type NHases, suggesting different mechanisms for the two types of NHases.

Synopsis: A strictly conserved active site αSer residue in both Co- and Fe-type nitrile hydratases was mutated. This αSer residue was found to play an important catalytic function, but is not essential. In Co-type NHases, it appears to be essential for active site maturation, but not in Fe-type NHases.

1. Introduction

Nitriles are common biological compounds that are used as a form of self-defense for many plants; however, nitriles also serve as building blocks for a variety of other compounds such as amides, aldehydes, and carboxylic acids [1–3]. For the conversion of nitriles to their corresponding amides, biology has evolutionarily developed a highly efficient metalloenzyme, nitrile hydratase (NHases, EC 4.2.1.84), that catalyzes the hydration of nitriles to amides. NHases are exceptional biocatalysts, with broad substrate selectivity but strict stereoselectivity, that are capable of hydrolyzing nitriles under mild reaction conditions to produce amides [4]. As such, they are in high demand as biocatalysts in preparative organic and pharmaceutical chemistry applications, as nitriles represent an important synthon that adds an extra carbon atom to an alkyl chain [5–7]. Due to the robust catalytic nature of NHases, these enzymes have now been exploited industrially [8,9] and are also being examined as a potential bioremediation catalyst of nitrile containing contaminants, as many nitriles have now made their way into ecosystems from their wide industrial use including the pesticide bromoxynil [10,11]. For further exploitation of the chemical potential of nitriles hydratases, a deeper understanding of the catalytic role of second-sphere active site residues is an important and necessary step.

* Corresponding author.
E-mail address: RHOLZ@MINES.EDU (R.C. Holz).

https://doi.org/10.1016/j.jinorgbio.2024.112763
Received 17 August 2024; Received in revised form 15 October 2024; Accepted 16 October 2024
Available online 18 October 2024

The most typical and hence extensively characterized prokaryotic NHases are α2β2 heterotetrameric holoenzymes. The α-subunit contains a highly conserved amino acid sequence (CXYCSCX) that contributes to a hexadentate metal binding active site composed of three cysteines (Cys, C), two backbone amide nitrogen atoms, and a water molecule (Fig. 1) [12]. The metal ion in the active site can be either a low-spin Fe (III) (S = 1/2) or a low-spin Co(III) (S = 0), depending on the source organism. The two equatorial active site cysteine residues are post-translationally oxidized to a Cys-sulfinic (-SO2(H), CSD) and Cys-sulfenic (-SO(H), CSO) acid for the enzyme to be functional (Fig. 1) [12,13]. If these cysteines are over- or under-oxidized, the enzyme is inactive [14,15]. A strictly conserved active site serine (Ser, S) residue forms a hydrogen bond (2.9 Å) to the active site water ligand (Fig. 1), as such it was hypothesized to play a role in catalysis. Previous mutation of this active site αSer residue to an alanine (Ala, A) in the Fe-type NHase from Rhodococcus erythropolis N771 (ReNHase-N771) reduced the observed catalytic activity by ~40 % [16].

NHases require the presence of an activator (ε) protein for metalation and functional expression [15,17,18]. While the Co-type and Fe-type NHase enzymes are largely similar in structure and sequence, their ε proteins are quite different. The Fe-type ε protein is ~45 kDa with a known CXCC metal binding motif and a Walker A/B motif indicative of a GTP binding site [17]. The Co-type ε protein, on the other hand, is much smaller, ~17 kDa, and has no known metal binding motifs nor does it contain a Walker A/B motif. Both the Fe- and Co-type ε proteins can function as GTPases, though the role GTP plays in NHase metalation and active site maturation is unknown [19,20]. A unique metal transfer mechanism was proposed for the Co-type ε protein, termed 'subunit swapping' [18,21,22]. In this process, one apo-α-subunit forms a complex with two metalated NHase ε proteins forming an $\alpha\varepsilon_2$ complex. The Co(II) ion is then proposed to be transferred to the α-subunit after which the Co(II) ion is oxidized to Co(III) followed by the two equatorial Cys ligands being oxidized to sulfenic and sulfinic acids [21]. Two highly conserved arginine (Arg, R) residues on the β-subunit are proposed to drive the subunit swapping process by forming a salt bridge with the equatorial oxidized Cys ligands [23]. It has been suggested that the Fe-type ε protein may also follow a subunit swapping process but forms a 1:1 αε complex [18,24].

To gain insight into the catalytic function and NHase metallocentre assembly and active site post-translational modification, the strictly conserved, second-sphere active site αSer112 residue in the Co-type NHase from *Pseudonocardia thermophila* JCM 3095 (*Pt*NHase) and the αSer117 in the Fe-type NHase from *Rhodococcus equi* TG328–2 (*Re*NHase) were mutated to Ala, aspartic acid (Asp, D) and threonine (Thr, T). Each of the *Pt*NHase and *Re*NHase mutant enzymes were characterized kinetically and spectroscopically; these data, coupled with X-ray crystal structures of the *Pt*NHase mutants, provide new insights into the catalytic mechanism of NHases and the proposed subunit swapping process [13,25–28].

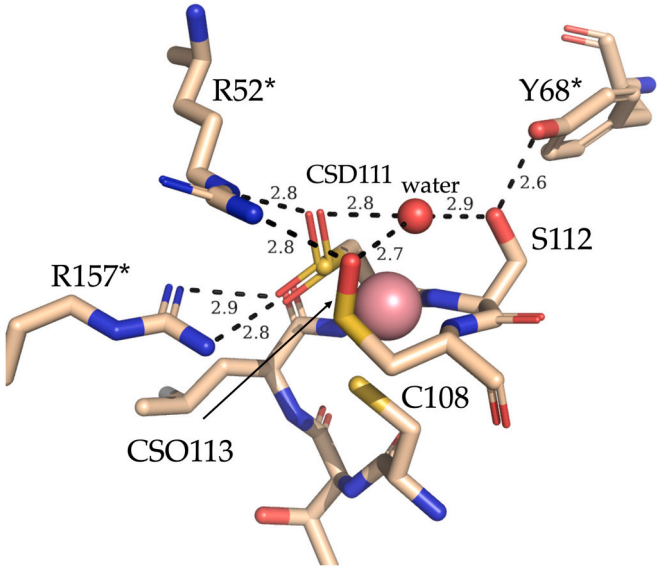

Fig. 1. Active site of WT *Pt*NHase (PDB: **1IRE**) where residues from the β subunit are denoted with *.

2. Materials and methods

2.1. Materials

Most materials and chemicals were purchased commercially at the highest purity available from either Sigma Aldrich or Fisher Scientific. Nickel nitriloacetic acid (Ni-NTA) columns (5 mL) were purchased from Qiagen. Pre-cast gels for sodium dodecyl sulfate–polyacrylamide gel (SDS-PAGE) electrophoresis, running buffers and protein ladders were purchased from Bio-Rad laboratories. Competent cells (XL10-Gold, NEB and BL21(DE3)) were purchased from Agilent Technologies along with QuikChange mutagenesis kits. Plasmid purification kits were purchased from Promega.

2.2. Mutagenesis

The two α/β subunits for both *Re*NHase and *Pt*NHase were previously inserted into a pET-28a(+) vector, as previously described [13]. The *Pt*NHase α subunit had an engineered His_6-tag on the C-terminus while *Re*NHase was engineered with two His_6-tags, one on the N-terminus of the α-subunit and the other on the C-terminus of the β-subunit. The following primers were designed to generate the desired mutants of the active site Ser residue (Integrated DNA Technologies) where the mutated codons are in lowercase here. The forward primer sequences are listed below and used with complementary reverse primer sequences.

- 5'-GTCGTGTGCACGCTCTGCgccTGCTAC-3' *Pt*NHase αS112A
- 5'-GTCGTGTGCACGCTCTGCgacTGCTACCCGTGG-3' *Pt*NHase αS112D
- 5'-GTCGTGTGCACGCTCTGCaccTGCTAC-3' *Pt*NHase αS112T
- 5'-TGCTCCCTCTGCacgTGCACAGCATGG3' *Re*NHase αS117A
- 5'-GTCTGCTCCCTCTGCgcgTGCACAGCA-3' *Re*NHase αS117T

Two half polymerase chain reactions (PCR) were performed for the forward and reverse reactions separately, and then mixed for further PCR. The mutated plasmids were then transformed into *XL10-Gold* competent cells and plated on kanamycin (50 μg/mL)/carbenicillin (100 μg/mL) agar plates. Colonies were selected and grown in LB broth under the same antibiotic conditions. These cultures were then used for the purification of each mutant plasmid using the Promega Wizard SV genomic DNA purification kit. Each plasmid was subsequently sequenced via GeneWiz for confirmation of the mutation. Plasmids were stored at −20 °C.

2.3. Expression and purification

Plasmids for the mutant *Pt*NHase and *Re*NHase enzymes were transformed into BL21(DE3) competent cells with the accompanying metallochaperone protein plasmid in a complementary vector, as previously described [23], and plated on kanamycin (50 μg/mL)/carbenicillin (100 μg/mL) agar plates. Single colonies were selected and grown in 100 mL of LB broth with 50 μg/mL kanamycin and 100 μg/mL ampicillin at 37 °C overnight at 200 rpm. This starter culture was then used to inoculate 8 L of LB broth containing kanamycin (50 μg/mL)/carbenicillin (100 μg/mL) at 37 °C until an OD_{600} between 0.8 and 1.0 was reached. Each flask was then induced with 0.1 mM isopropyl-β-D-1-

thiogalactopyrranoside (IPTG), cooled to 20 °C, and shaken at 200 rpm for 16 h. In the cultures of *Pt*NHase, 0.25 mM cobalt chloride was added. Cell cultures were harvested via centrifugation at 5000 × *g* for 15 min and the pelleted cells were resuspended in 'Buffer A' (50 mM HEPES, 500 mM NaCl at pH 7.5 filtered through a 0.22 μm nitrocellulose membrane). These cells were lysed on ice via sonication (Misonix Sonicator 300 with microtip) in 45 s increments for 20 min at 21 W. The cell debris and soluble protein were separated via centrifugation for 45 min. at 10,000 × *g*.

The supernatant for each mutant *Pt*NHase or *Re*NHase enzyme was loaded onto a pre-packed 5 mL immobilized-metal affinity chromatography (IMAC) nickel-nitrilotriacetic acid (Ni-NTA) column (QIAGEN) connected to an ÄKTA Prime Plus FPLC system that was previously equilibrated with Buffer A (50 mM HEPES, 500 mM NaCl, pH 7.5 containing 40 mM butyric acid) that had been vacuum filtered through a 0.22 μm nitrocellulose filter [26]. The column was washed with 20 column volumes (CV) of Buffer A, and the His_6-NHase was eluted with a linear gradient (0–100 %) using a high imidazole content Buffer B (50 mM HEPES, 500 mM NaCl, 500 mM imidazole, pH 7.5 containing 40 mM butyric acid) at a flow rate of 1 mL/min. Fractions containing the His_6-NHase protein were collected, and buffer exchanged into Buffer A and concentrated using a 30 kDa Amicon centrifugation tube. Each His_6-NHase protein was shown to be pure via SDS-PAGE (12.5 %).

2.4. Metal content and kinetic analysis

Metal analysis was performed via inductively coupled plasma atomic emission spectroscopy (ICP-AES). Each mutant His_6-NHase protein sample was denatured in 8 M urea and acidified with 2 % nitric acid and 0.5 % hydrochloric acid *v*/v mixture to a final volume of 10 mL, as previously described (Table 1) [23]. After 24 h, the digested protein samples were filtered using 0.2 μM syringe filters and submitted, along with a control of buffer containing no protein, for analysis.

The enzymatic activity of each NHase mutant was determined utilizing acrylonitrile as the substrate and monitoring the production of acrylamide ($\Delta\varepsilon_{225} = 2.9\ mM^{-1}\ cm^{-1}$) on an Agilent 8453 UV–visible spectroscopy system equipped with an Agilent 89090 A Peltier temperature-controlled cell holder. The 1 mL reaction mixture comprised 0.5–60 mM acrylonitrile and 100–200 nM of the enzyme being tested in 50 mM Tris-HCl buffer at pH 7.5 and 25 °C. OriginPro9.0 software was used to fit these data to Michaelis-Menten kinetics parameters k_{cat} and K_M.

Table 1
Kinetic constants and metal equivalents (eqs.) for each WT and mutant protein for the conversion of acrylonitrile to acrylamide in 20 mM Tris-HCl at pH 7 under 25 °C. M^{3+} = Fe(III) for *Re*NHase species and M^{3+} = Co(III) for *Pt*NHase species.

	k_{cat} (s^{-1})	K_M (mM)	k_{cat}/K_M (s^{-1} mM^{-1})	M^{3+} eqs.
WT *Re*NHase	1300 ± 200	31 ± 1	42	2.0 ± 0.1
*Re*NHase αSer117Ala	93 ± 3	12 ± 4	8	1.7 ± 0.2
*Re*NHase αSer117Thr	40 ± 2	4 ± 1	10	1.0 ± 0.2
WT *Pt*NHase	1600 ± 120	7 ± 1	300	2.0 ± 0.1
*Pt*NHase αSer112Ala	0.20 ± 0.02	7 ± 4	0.03	0.04 ± 0.01
*Pt*NHase αSer112Asp	0.13 ± 0.01	8 ± 2	0.02	0.08 ± 0.02
*Pt*NHase αSer112Thr	0.03 ± 0.01	11 ± 4	0.003	0.08 ± 0.02

2.5. Absorbance spectroscopy and electron paramagnetic resonance (EPR) spectroscopy

Each mutant was concentrated to ~300 μM per homodimer in 50 mM HEPES buffer at pH 7.5 before spectroscopic measurements. Absorbance spectra were collected on a Shimadzu UV-2600i with a T2X2 dual temperature controller in a 1 cm path length quartz cuvette at 25 °C. X-band EPR spectra were obtained on a Bruker EMX-AA-TDU/L spectrometer with a Bruker ER 4103TM cavity, resonant at 9.45 GHz at 77 K, and using 2 G magnetic field modulation at 100 kHz [20]. Spectral analysis and simulations were performed using EasySpin [29].

2.6. X-ray crystallography

Crystallization of the *Pt*NHase mutant enzymes were performed using a sitting drop protocol of 20 mg/mL protein solution mixed with a well solution consisting of 1.2 M sodium citrate tribasic in 0.1 M HEPES at pH 7.5, as previously reported [12,23]. Diffraction quality, colorless crystals for each *Pt*NHase mutant grew within two weeks and upon harvesting, were frozen in a cryoprotectant containing the crystallization buffer and 20 % glycerol (*v*/v). X-ray diffraction data were collected at the Stanford Synchrotron Radiation Lightsource (SSRL) on beamline 9–2 with a Dectris Pilatus 6 M PAD detector. Data were collected over a range of (360°), an oscillation angle of 0.2°, an exposure time of 1 s and wavelength was fixed at 0.979460 Å. Data were processed, integrated, indexed and scaled using AutoXDS [30]. The Phenix software suite was used to perform molecular replacement and refinement for each *Pt*NHase mutant structure using the previously published WT *Pt*NHase (PDB: **1IRE**) [31]. Figures were created with PyMOL and detailed processing statistics are listed in Table 3. [32].

3. Results and discussion

In all Fe- and Co-type NHases, a highly conserved, second-sphere, active site αSer residue (αSer112 in *Pt*NHase and αSer117 in *Re*NHase) forms a hydrogen-bond, ~2.9 Å, to the axial water ligand of the active site trivalent metal ion (Fig. 1) [12]. This αSer residue is part of the highly conserved amino acid sequence (CXYCSCX) that makes up the NHase active site where its backbone amide nitrogen is an active site ligand. It has been shown that the carbon–nitrogen bonds of this coordinated amide have significant double bond character, suggesting it is best represented as imido-metal bond [33]. In both *Pt*NHase and *Re*NHase, this second-sphere αSer residue also forms a hydrogen bond with a βTyr residue, which is conserved within most Co- and Fe-type NHases [16]. Previously, this αSer residue was mutated to Ala in the Fe-type NHase from *Rhodococcus erythropolis* N771 (*Re*NHase-N771), and the resulting NHase exhibited catalytic activity that was reduced by ~40 % [16]. Even so, the catalytic role of this αSer residue is not well understood, nor is it known if this αSer residue is involved in NHase metallocentre assembly and active site post-translational modification. Given that this residue is strictly conserved within the NHase active site, it was substituted by Ala, Asp and Thr in *Pt*NHase and Ala and Thr in *Re*NHase.

3.1. Purification, metal analysis and kinetic parameters

Each mutant was successfully expressed and purified as previously reported for WT *Re*NHase or WT *Pt*NHase and shown to be pure via SDS-PAGE (12.5 %). The mutant enzymes (*Re*NHase αSer117Ala, *Re*NHase αSer117Thr, *Pt*NHase αSer112Ala, *Pt*NHase αSer112Asp, and *Pt*NHase αSer112Thr) each exhibited diminished metalation, with <0.08 eqs. of cobalt per tetramer for each *Pt*NHase mutant while *Re*NHase αSer117Ala retained 1.7 ± 0.2 eqs. of iron per tetramer and *Re*NHase αSer117Thr contained 1.0 ± 0.2 eqs. per tetramer (Table 1). As the metal content for the three *Pt*NHase mutants was <4 % of that observed for WT *Pt*NHase, mutation of the second-sphere αSer residue clearly impacts the ability of

the active sites to incorporate metal ions, suggesting that this αSer residue may play a role in the subunit swapping process observed for Co-type NHases. On the other hand, the *Re*NHase mutants contained between 50 and 85 % of the WT metal content, suggesting a different and limited role in the metalation process for Fe-type NHases [16].

The catalytic constants for WT and each of the mutant NHases are presented in Table 1. The *Pt*NHase mutants displayed significantly diminished k_{cat} values, with *Pt*NHase αSer112Ala, *Pt*NHase αSer112Asp, and *Pt*NHase αSer112Thr exhibiting k_{cat} values between 0.03 ± 0.01 and 0.2 ± 0.02 s^{-1}, compared to WT *Pt*NHase, which exhibits a k_{cat} of 1600 ± 120 s^{-1} (Table 1). The K_M values for each of the *Pt*NHase mutant enzymes were found to be between 7 ± 4 and 11 ± 4 mM, which were indistinguishable from WT *Pt*NHase (~7 ± 1 mM) (Table 1). As a result of the decreased k_{cat} values, the catalytic efficiency (k_{cat}/K_M) for each *Pt*NHase mutant enzyme decreased >3000-fold (Table 1). As the substrate has been shown to directly bind to the active site metal ion, the diminished catalytic activity is likely directly related to the >95 % decrease active site Co(III) ions.

The observed k_{cat} values for the *Re*NHase αSer117Ala and αSer117Thr mutant enzymes were 93 ± 3 and 40 ± 2 s^{-1}, compared to WT *Re*NHase, which exhibits a k_{cat} of 1300 ± 200 s^{-1} (Table 1). The K_M value for *Re*NHase αSer117Thr was 4 ± 1 mM while αSer117Ala exhibited a K_M value of 12 ± 4 mM, both of which are somewhat lower than the K_M value for WT *Re*NHase of 31 ± 1 mM (Table 1). Consequently, the catalytic efficiency (k_{cat}/K_M) for each *Re*NHase mutant enzyme was approximately four-fold lower than for WT *Re*NHase (Table 1). Mutation of the αSer113 to an Ala residue in *Re*NHase-N771, resulted in a mutant enzyme that retained ~60 % of its catalytic activity, however, no metal analysis was reported [16]. These data suggest that the hydrogen bonding interaction between the αSer residue and the axial water ligand plays an important role in catalysis, likely by maintaining the axial ligand as a water molecule and not a hydroxide, as hydroxide would be more difficult to displace by the incoming R-CN substrate. The αSer may also play a role in stabilizing the proposed cyclic intermediate that forms after nucleophilic attack of the equatorial bound nitrile carbon by the sulfenic acid ligand [12,13]. Even so, as both *Re*NHase mutants as well as those from *Re*NHase-N771 retained a significant amount of active site Fe(III) ions and activity, the conserved active site αSer117 residue, while important for catalysis, is not required.

3.2. Electronic absorption and electron paramagnetic resonance spectroscopy

The UV–Vis spectrum of WT *Pt*NHase exhibited a characteristic band at 320 nm due to an axial thiolate S(π)-to-Co(III) ligand-to-metal charge transfer (LMCT) transition (Fig. 2). As a result, the sample exhibited an observable tan (straw) color [27,34]. Under the same conditions, all three of the *Pt*NHase αSer112 mutants were colorless and had no observable axial thiolate S(π)-to-Co(III) charge transfer (CT) transitions (Fig. 2). The diminution of this LMCT band is likely the result of low Co (III) content in each mutant enzyme. Conversely, the UV–Vis spectra of *Re*NHase αSer117Ala exhibited an axial thiolate S(π)-to-Fe(III) LMCT transition at ~710 nm, which was red-shifted compared to the *Re*NHase αSer117Thr mutant enzyme and WT *Re*NHase, both of which exhibited this LMCT band at ~690 nm (Fig. 3). Given the similarity in sidechains between Ser and Thr, a similar position of this LMCT is not unexpected. It should be noted that the molar absorptivity at 690 nm for the αSer117Thr mutant is ~75 % smaller compared to WT *Re*NHase, which could reflect the methyl group on the Thr side chain resulting in a steric effect for hydrogen bond formation to the axial water ligand or due to the 50 % reduction in metalation observed for this enzyme. The ~20 nm red-shift observed in the LMCT band for *Re*NHase αSer117Ala indicates a change in the electronic environment around the active site Fe(III) ion likely due to the lack of a hydrogen bond from the αSer. Two other absorption bands at ~375 and ~ 450 nm, which were previously assigned as S(π)-to-Fe(III) LMCT bands, were observed for *Re*NHase

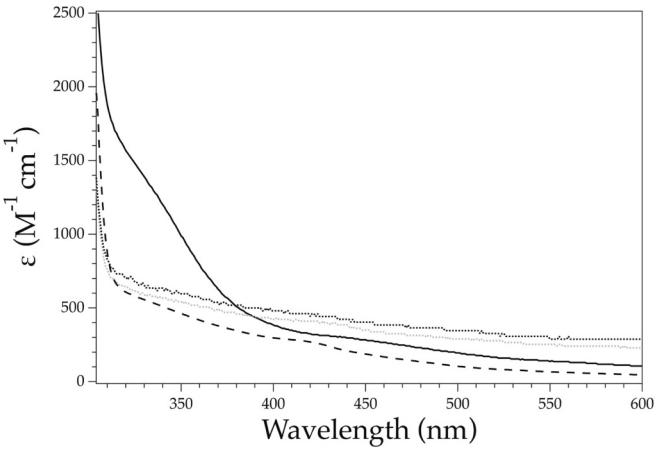

Fig. 2. Absorption spectra of WT *Pt*NHase (solid black trace), *Pt*NHase αSer112Ala (black long dash trace), *Pt*NHase αSer117Asp (black dotted trace) and *Pt*NHase αSer117Thr (gray dotted trace) in 50 mM HEPES at pH 7.5 at 25 °C.

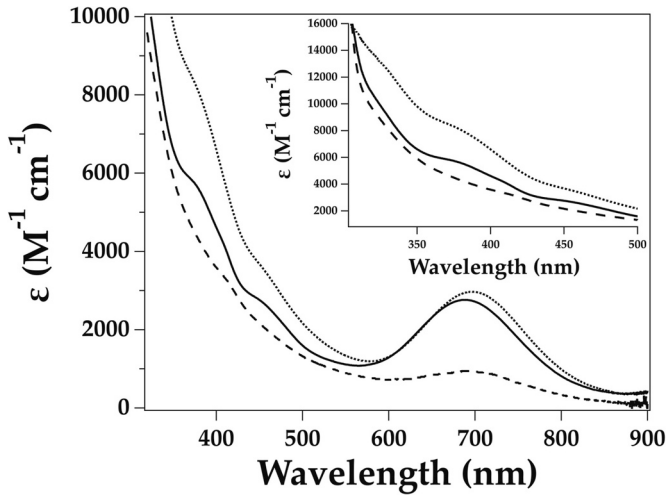

Fig. 3. Absorption spectra normalized to protein concentrations for WT *Re*NHase (solid black trace), *Re*NHase αSer117Ala (black dotted trace, ~85 % metalation) and *Re*NHase αSer117Thr (black long dash trace, ~50 % metalation).

αSer117Ala but are not clearly observed for *Re*NHase αSer117Thr, likely due to the ~50 % decrease in metalation (Fig. 3, inset) [26].

The UV–Vis spectra obtained for *Re*NHase αSer117Ala and αSer117Thr are similar to those reported for the αSer113Ala mutant *Re*NHase-N771 enzyme [16]. The axial ligand in *Re*NHase-N771 αSer113Ala was found to be nitroxide instead of water, resulting in an inactive enzyme that could be photoactivated via denitrosylation. Upon denitrosylation, *Re*NHase-N771 αSer113Ala was found to be very air sensitive so the characteristic S(π)-to-Fe(III) LMCT at ~690 nm was not observed; photoactivated *Re*NHase-N771 αSer113Ala was, however, stabilized by the presence of butyric acid (BA). Similar to the UV–Vis spectra obtained for *Re*NHase αSer117Ala and αSer117Thr, mutation of the conserved active site αSer residue to an Ala residue in *Re*NHase-N771 affected the electronic environment of the active site Fe(III) ion [16]. Combination of these data with those obtained for *Re*NHase αSer117Ala and αSer117Thr indicates that the conserved active site αSer residue impacts the active site through hydrogen bond formation with the axial water ligand and likely assists to tune the Lewis acidity of the active site metal ion [35].

EPR spectra of the WT and mutated forms of *Re*NHase are presented

in Fig. 4. WT *Re*NHase EPR spectra typically contain three distinct species: active enzyme (*Re*NHase^{Aq}) with g_1 = 2.206, oxidized enzyme (*Re*NHase^{Ox}) with g_1 = 2.180, and BA bound (*Re*NHase^{BA}) with g_1 = 2.281 (Table 2) [23,36]. EPR spectra obtained for the *Re*NHase αSer117Ala and αSer117Thr mutant enzymes were prepared without the addition of butyric acid eliminating one of the species typically observed for WT *Re*NHase. For *Re*NHase αSer117Ala, two overlapping signals were observed at 3113 G and 3150 G that were assigned to the *Re*NHase^{Aq} αSer117Ala (g_1 = 2.213) and the *Re*NHase^{Ox} αSer117Ala (g_1 = 2.189), which yields a Δ*g* of ~0.007 and 0.009 from WT *Re*NHase, respectively. This fairly significant shift in g_1 is indicative of an altered electronic environment around the low-spin Fe(III) ion. Additionally, the *Re*NHase^{Ox} αSer117Ala signal intensity is more intense than the *Re*NHase^{Aq} αSer117Ala, due to the lack of BA in the sample.

The EPR spectrum of *Re*NHase αSer117Thr also revealed two species at 3108 G and 3140 G that were assigned to the *Re*NHase^{Aq} αSer117Thr (g_1 = 2.218) and the *Re*NHase^{Ox} αSer117Thr (g_1 = 2.199) enzyme (Table 2). Comparison of these data to the WT *Re*NHase g_1 values revealed a Δ*g* of ~0.012 and 0.019, an even larger shift than observed for the Ala mutant. The relative intensities of the two signals observed for in the *Re*NHase αSer117Thr EPR spectrum are opposite that observed for the *Re*NHase αSer117Ala mutant in that the *Re*NHase^{Aq} αSer117Thr is more intense than the *Re*NHase^{Ox} αSer117Thr signal, suggesting that the *Re*NHase αSer117Thr mutant enzyme is less susceptible to air oxidation than the *Re*NHase αSer117Ala mutant enzyme. Additionally,

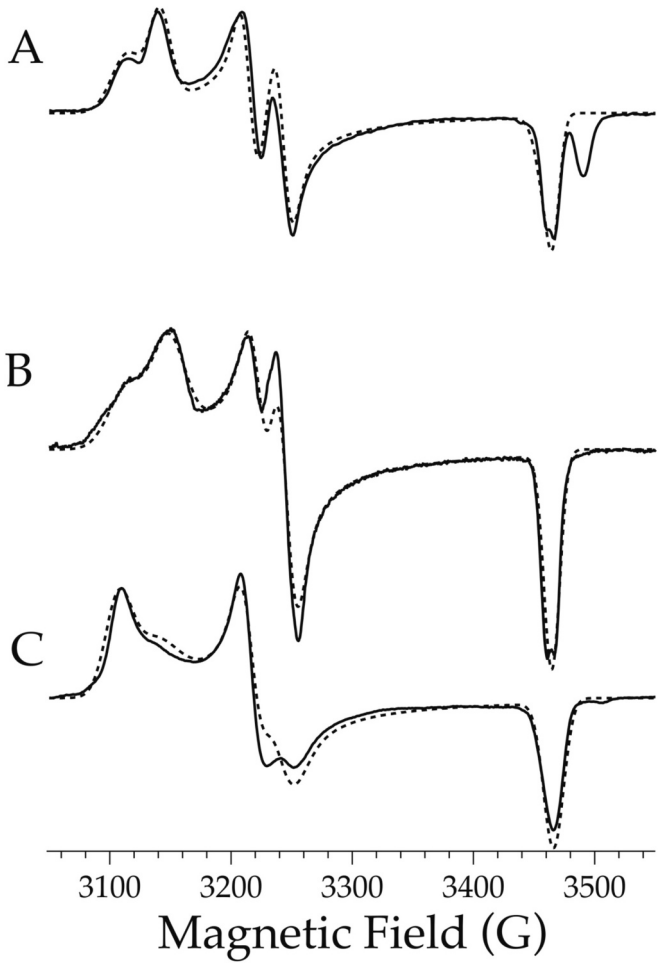

Fig. 4. X-band EPR spectra of the WT *Re*NHase, simulated without the signal due to butyric acid (A), *Re*NHase αSer117Ala (B), and *Re*NHase αSer117Thr (C) where experimental spectra are shown in black solid line and simulated spectra overlaid in the black dashed line, collected in 50 mM HEPES at pH 7.5 at 77 K with the field centered at 9.644 G at 2 mW.

Table 2
Experimental *g* values for WT *Re*NHase, *Re*NHase αSer117Ala and *Re*NHase αSer117Thr.

	g_1	g_2	g_3	g_1-g_3
WT *Re*NHase^{Aq}	2.206	2.131	1.987	0.219
WT *Re*NHase^{Ox}	2.180	2.114	1.998	0.182
*Re*NHase^{Aq} αSer117Ala	2.213	2.138	1.987	0.226
*Re*NHase^{Ox} αSer117Ala	2.189	2.123	1.990	0.199
*Re*NHase^{Aq} αSer117Thr	2.218	2.142	1.986	0.232
*Re*NHase^{Ox} αSer117Thr	2.198	2.128	1.990	0.209

EPR spin signal quantitation revealed ~1.5 eq Fe(III) for *Re*NHase αSer117Ala and ~ 0.6 eq Fe(III) for *Re*NHase αSer117Thr when compared to WT, which is in excellent agreement with ICP-MS data which revealed 1.7 ± 0.2 eq for the Ala mutant and 1.0 ± 0.2 eq for the Thr mutant. Thus, the low activity for these mutants is not solely due to low iron in the active site. These data agree with the UV–Vis data as they reflect a change in the electronic environment of the active site Fe(III) ion, consistent with the conserved active site αSer residue playing a role in tuning the active site metal ion.

3.3. Crystallography

X-ray quality crystals of each of the *Pt*NHase αSer112 mutant enzymes were obtained using identical crystallization conditions to those previously reported for WT *Pt*NHase [13,23]. Each crystal was colorless, consistent with the low metal content detected via ICP-AES (Table 1). Crystals of the *Pt*NHase αSer112Ala (PDB: **9D5U**), αSer112Asp (PDB: **9D5V**), and αSer112Thr (PDB: **9D5Y**) mutant enzymes diffracted between ~1.26 and 1.35 Å, with complete statistics presented in Table 3. All three of the X-ray structures confirm the mutations and their overall structures were nearly identical to that of WT *Pt*NHase with an RMSD ranging from ~0.214 to 0.299 Å. The active sites for each of the *Pt*NHase αSer112 mutant enzymes are presented in Figs. 5A-C. No metal density

Table 3
Refinement and data collection statistics for each *Pt*NHase mutant crystal structure, with PDB codes shown in parenthesis.

Data Set	αS112A (9D5U)	αS112D (9D5V)	αS112T (9D5Y)
Space Group	$P3_221$	$P3_221$	$P3_221$
Cell Dimensions			
a = b (Å)	65.84	65.68	65.93
c (Å)	185.64	185.14	185.78
α = β (°)	90	90	90
γ (°)	120	120	120
Resolution (Å)	32.92–1.35	32.84–1.26	36.03–1.35
R_{merge}	0.034 (0.470)	0.011 (0.258)	0.014 (0.396)
R_{pim}	0.034 (0.470)	0.011 (0.258)	0.014 (0.396)
I/sigma	7.50 (1.01)	18.86 (1.83)	13.07 (1.01)
Completeness (%)	97.60 (85.20)	99.91 (99.85)	98.36 (83.77)
Multiplicity	2.0 (2.0)	2.0 (2.0)	2.0 (2.0)
No. Total reflections	200,813 (17256)	251,194 (24539)	204,132 (17202)
No. Unique reflections	100,939 (8715)	125,645 (12297)	102,066 (8601)
R_{work}	0.239 (0.334)	0.213 (0.279)	0.232 (0.318)
R_{free}	0.259 (0.321)	0.230 (0.289)	0.257 (0.322)
Twin Law	-h,-k,l	-h,-k,l	-h,-k,l
No. of Atoms	3727	3808	3741
No. of Solvent Atoms	215	335	269
B-factors (Å^2)			
Overall	18.63	16.37	21.57
Protein	18.57	16.16	21.43
Water	19.31	18.50	23.18
RMSD Bond Length (Å)	0.020	0.008	0.008
RMSD Bond Angles (°)	2.05	0.98	1.08
Ramachandran			
Favored (%)	97.87	98.10	97.16
Allowed (%)	1.66	1.90	2.84
Outlier (%)	0.47	0.00	0.00

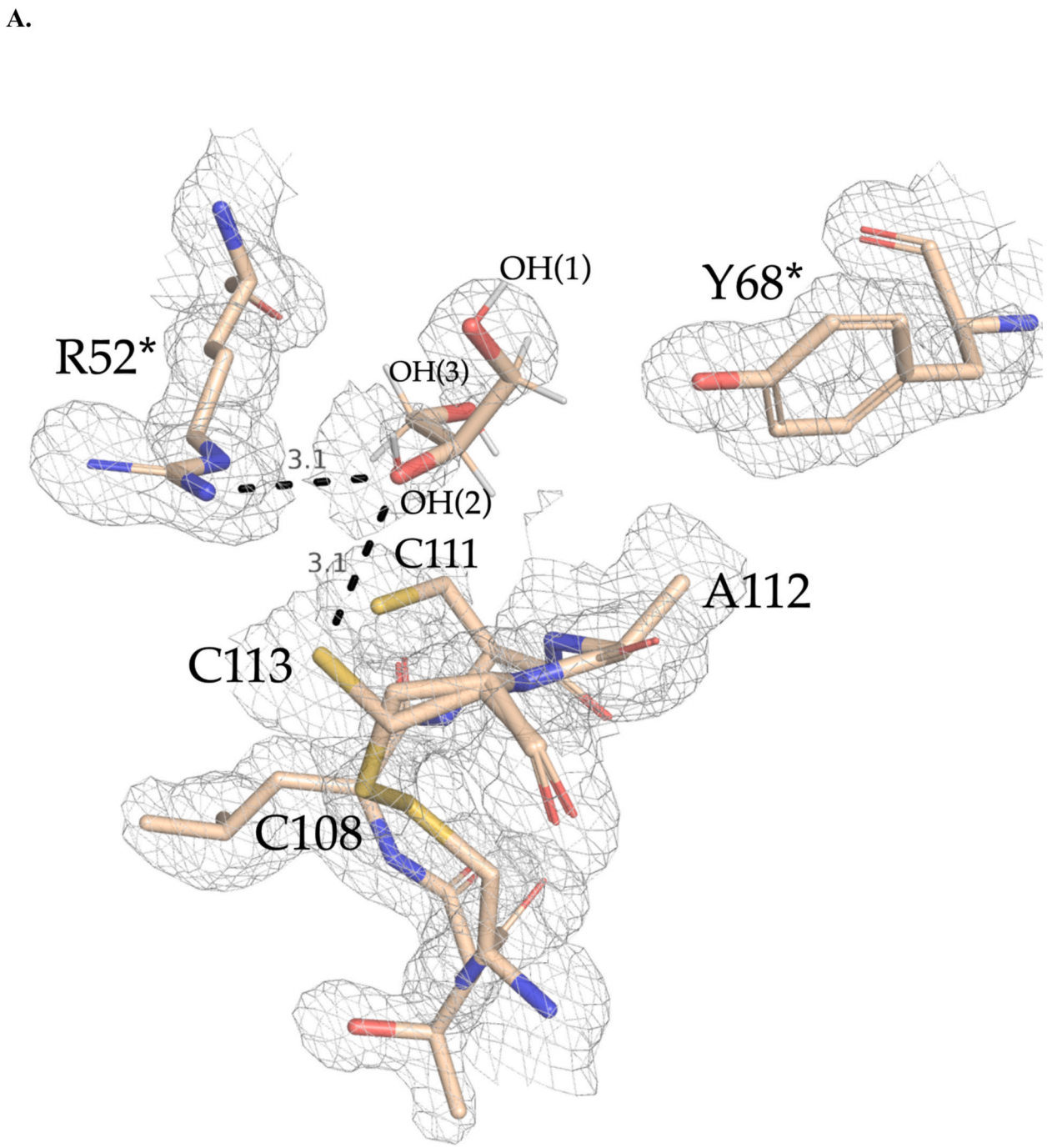

Fig. 5. A) Active site of *Pt*NHase αSer112Ala (PDB: **9D5U**) with the polder map at sigma 1.0 level shown in gray mesh **B).** Active site of *Pt*NHase αSer112Asp (PDB: **9D5V**) with the polder map at sigma 1.0 level shown in gray mesh and **C).** Active site of *Pt*NHase αSer112Thr (PDB: **9D5Y**) with the polder map at sigma 1.0 level shown in gray mesh (residues from the β subunit are denoted with *).

was observed in any of the active sites, so the collected data was solved as the apo-form; however, densities less than 20 % are often poorly resolved via X-ray crystallography so we cannot exclude the possibility of low metal occupancy in the active site.

In the *Pt*NHase αSer112Ala structure, the active site equatorial cysteine ligands αC111 and αC113 are fully reduced with the αCys113 residue occupying two conformations in a 50:50 ratio (Fig. 5A). A disulfide bond likely exists between the αCys108 and αCys113 residues (2.1 Å) in one of the confirmations, similar to that observed in the apo-*Pt*NHase X-ray structure (PDB: **1UGQ**) (Table 4) [37]. As with *Pt*NHase αSer112Ala, the active site equatorial cysteine ligands αC111 and αCys113 are also fully reduced in the *Pt*NHase αSer112Asp mutant structure (Fig. 5B). Both active site cysteine residues in the *Pt*NHase αSer112Asp structure reside in only one conformation and no disulfide bond is observed between αCys113 and αCys108 (3.8 Å). Interestingly, in *Pt*NHase αSer112Thr, the active site αCys113 residue is oxidized to a sulfenic acid (αCysSO113) while the αCys111 active site residue was fully reduced. Moreover, each active site Cys residue in the *Pt*NHase αSer112Thr structure occupied only one conformation with αCys111 and αCys108 possibly forming a weak disulfide bond (3.6 Å) as the van der Waals radius of S^{-} is 1.8 Å (Table 4). These data suggest that the active site αSer residue in *Pt*NHase likely plays a role in the post-

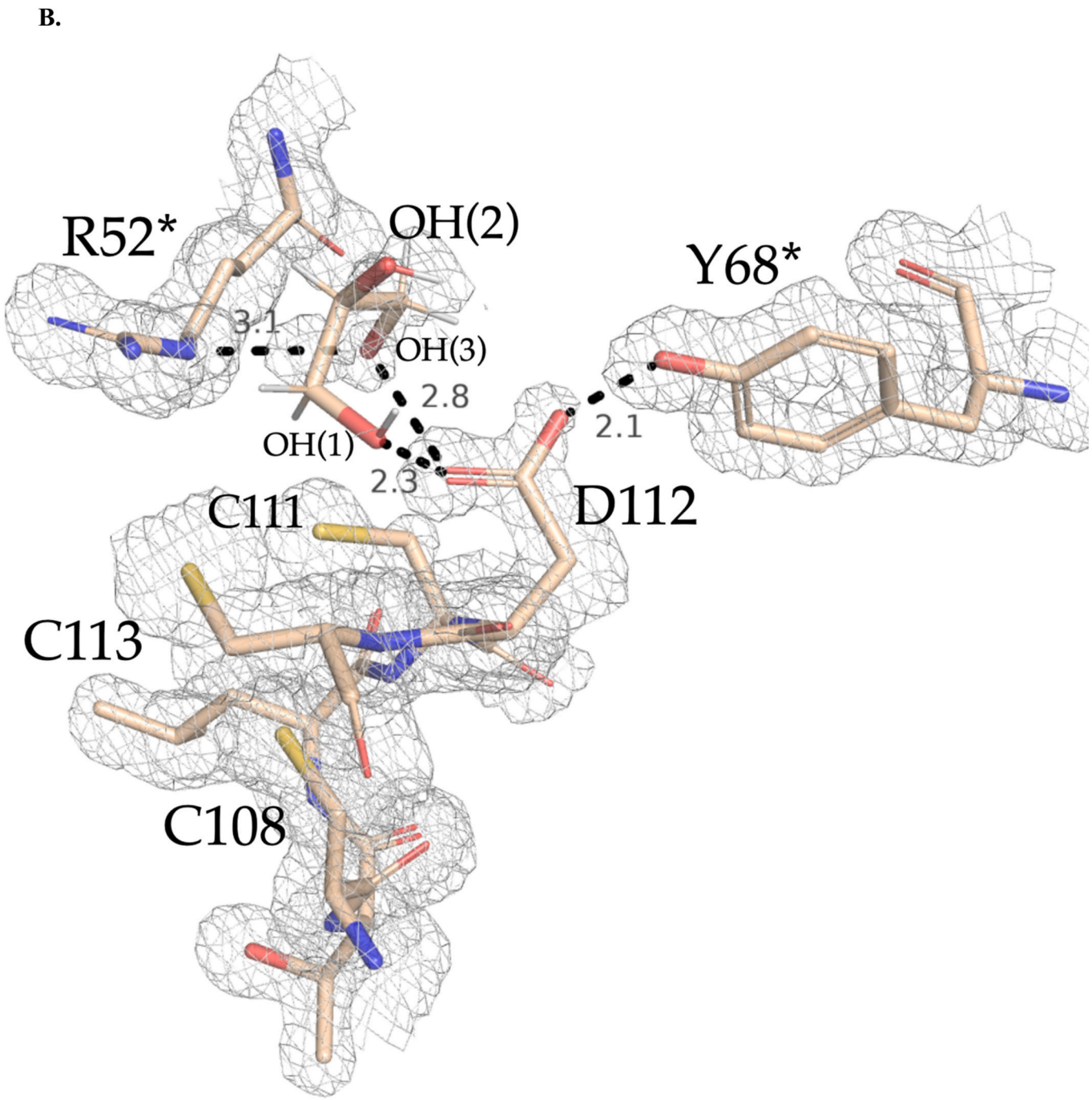

Fig. 5. (*continued*).

translational modification of the NHase active site as its absence impedes active site maturation, including metal ion insertion, and consequently subunit swapping. It is also possible, perhaps probable, that the correct post translational modification requires the proper incorporation of metal, which is disrupted by the mutation to the αSer residue. As the αSer residue clearly disrupts metal loading in the Co-type, perhaps the incorporation of metal precedes the oxidation of the cysteines [25]. These data further support the hypothesis that the proposed subunit swapping mechanism is different in Co- and Fe-type NHases, respectively, likely due to the very different ε proteins for Fe- vs Co-type NHases.

In WT *Pt*NHase (PDB: **1IRE**), the αSer112-OH group is positioned 2.6 Å from the -OH of βTyr68 (Fig. 1; Table 4). βTyr68 has previously been proposed to participate in catalysis as this hydrogen bond to the αSer112-OH group was suggested to modulate its ability to form a hydrogen bond to the active site axial water molecule. The second sphere βTyr68 residue has also been proposed to assist in substrate binding as a hydrogen bonding interaction was observed between the -OH group of βTyr68 and an oxygen atom of butyric acid (PDB: **1UGP**) [37]. Additionally, computational studies suggested that the αSer112-OH group can accept a proton from a water molecule, something that has not been verified experimentally [38]. Comparison of the *Pt*NHase structure with the three *Pt*NHase αSer mutant structures reveal hydrogen bonding interactions in *Pt*NHase αSer112Asp and αSer112Thr with the βTyr68-OH group (Figs. 5A-C; Table 4). In *Pt*NHase αSer112Thr, the bond distance between the αThr112-OH group and the βTyr68-OH group is 2.3 Å, which is shorter than the hydrogen bond distance observed in WT *Pt*NHase (2.6 Å). In *Pt*NHase αSer112Asp, the

C.

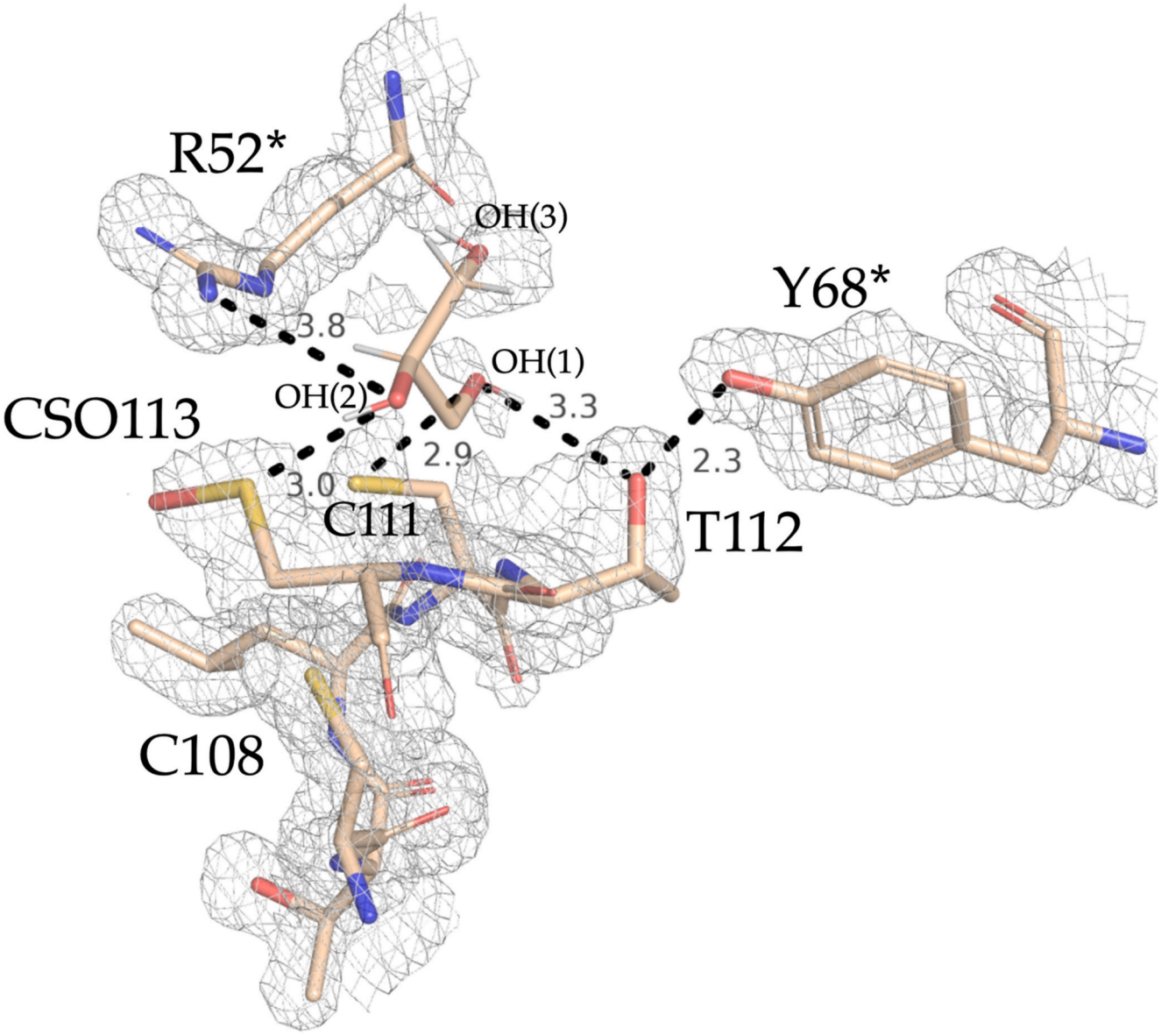

Fig. 5. (*continued*).

Table 4
Hydrogen bonding distances between first- and second-sphere ligands and glycerol with distances in Å.

	Species			
Bonds	WT	S112A	S112D	S112T
C108 – C113	3.1	2.1	3.8	3.9
C108 – C111	3.3	3.5	3.7	3.6
S/D/T112 -OH – Y68	2.6	–	2.1	2.3
R52 Secondary NH_2 – Glycerol OH(3)	–	–	3.1	–
R52 Primary NH_2 – Glycerol OH(2)	–	3.1	–	3.8
C113 – Glycerol OH(2)	–	3.1	–	3.0
C111 – Glycerol OH(3)	–	3.6	3.5	2.9
D112 – Glycerol OH(3)	–	–	2.8	–
D112 – Glycerol OH(1)	–	–	2.3	–
T112 – Glycerol OH(3)	–	–	–	3.3

αAsp112 hydrogen bonding distance to the βTyr68-OH group is only 2.1 Å, likely due to the negative charge associated with the αAsp112 group.

Finally, in each *Pt*NHase αSer112 mutant enzyme structure, clear density was observed above the active site in the potential substrate binding pocket (Figs. 5A-C). This observed density could be reasonably fit to a glycerol molecule, which was present as a cryoprotectant. In the *Pt*NHase αSer112Ala structure, the glycerol OH(2)-group is 3.1 Å from the terminal N atom of βArg52 suggesting a hydrogen bonding interaction (Figs. 5A, Table 4). The OH(2)-group of the glycerol molecule is also 3.1 Å from one conformation of the αC113-S atom, suggesting a weak hydrogen bonding interaction. In the *Pt*NHase αSer112Asp structure, the orientation of the glycerol molecule is altered in that the glycerol OH(3)-group now forms a hydrogen bond with the secondary amine N atom of βArg52 (3.1 Å) (Figs. 5B). The glycerol OH(1)-group has rotated and is now close to the O atoms of αAsp112 residue (2.3 Å), and the OH(3)-group is 2.8 Å from the O atom of αAsp112. This

altered glycerol binding mode places the glycerol OH(3)-group >4.5 Å from the βTyr68-OH group so no hydrogen bonding interaction is present (Table 4). In the *Pt*NHase αSer112Thr structure, yet another glycerol orientation exists (Figs. 5C). In this structure, the glycerol is closer to the active site ligands resulting in a relatively weak hydrogen bonding interaction between the glycerol OH(2)-group and the terminal βArg52 N atom (3.8 Å) [39]. The glycerol OH(1)-group is 3.3 Å from the -OH of αThr112 and 2.9 Å from the S atom of the reduced αCys111 residue. The glycerol OH(2)-group is 3.0 Å from the S atom of the αCysSO113, which functions as the nucleophile in the catalysis. Similarly to the Asp mutant, this altered glycerol binding mode places the glycerol OH(3)-group >4.5 Å from the βTyr68-OH group so no hydrogen bonding interaction is present. These data are consistent with βArg52 proposed role of facilitating substrate binding [23]. The three observed glycerol orientations are also consistent the substrate binding steps observed in time-resolved crystallographic data for the *Re*NHase-N771 enzyme using *tert*-butylisonitrile (*t*BuNC) as the substrate [14,40]. These time-resolved X-ray data showed a progression of *t*BuNC density in the active site, where it changes orientation over time to finally settle near the αCysSO113 residue, positioned for nucleophilic attack. Herein, a similar progression is observed (Fig. 5) as the glycerol molecule is seen in several different conformations, including a conformation where it is close (3.0 Å) to the catalytic nucleophile, αCysSO113.

4. Conclusions

The data described herein suggest a role for the conserved active site αSer residue in the subunit swapping process for Co-type NHases and the subsequent post-translational maturation of the active site. However, the second-sphere αSer residue in Fe-type NHases, while catalytically important, is not required and does not appear to play a significant role in metallocentre assembly and active site post-translational modification. Therefore, it appears that the subunit swapping mechanisms for Co- vs Fe-type NHases are different, which is consistent with the lack of any sequence similarity between the Co- and Fe-type NHase ε proteins. Additionally, these data support the previously proposed catalytic mechanism for NHases and are consistent with the recently updated proposed catalytic mechanism that includes two conserved second-sphere βArg residues (Fig. 6). Salient features of the proposed mechanism that remain the same include (i) direct coordination of the nitrile substrate to the active site metal center activating the nitrile bond towards nucleophilic attack, (ii) nucleophilic attack of the bound nitrile carbon by the sulfenic acid ligand, forming a cyclic intermediate, and (iii) the transfer of two protons upon product release, which is the rate-limiting step based on kinetic isotope studies [26,41]. Inclusion of the αSer residue in the proposed catalytic mechanism reveals a hydrogen bond to the axial water ligand in the resting enzyme, which also forms hydrogen bonds with both the sulfenic and sulfinic acid ligands. After nucleophilic attack, once the cyclic intermediate is formed, tautomerization occurs to form the iminol, which is likely stabilized by hydrogen bond formation with the αSer residue. As the αSer residue is not essential in catalysis, in its absence an active site water molecule may function as a hydrogen bonding partner. The cyclic catalytic intermediate necessitates stabilization of a reduced αCys113 ligand, which has been proposed to occur either through a disulfide bond intermediate or through a water molecule that reforms the sulfenic-αCys113 ligand (shown through red hashed lines in Fig. 6) [27]. The suggested disulfide intermediate has only been proposed from theoretical studies. Time-resolved X-ray crystallographic studies failed to detect a disulfide species, and mutation of the axial Cys ligand to His, which cannot form a disulfide bond, resulted in active enzyme [27]. Therefore, the formation of a disulfide bond between the axial Cys ligand and the equatorial sulfenic acid is not catalytically required. However, a recent EPR study reported a catalytically relevant intermediate that was tentatively assigned to a possible disulfide intermediate [42]. Finally, the αSer residue likely assists in amide product release, which likely occurs concurrently with

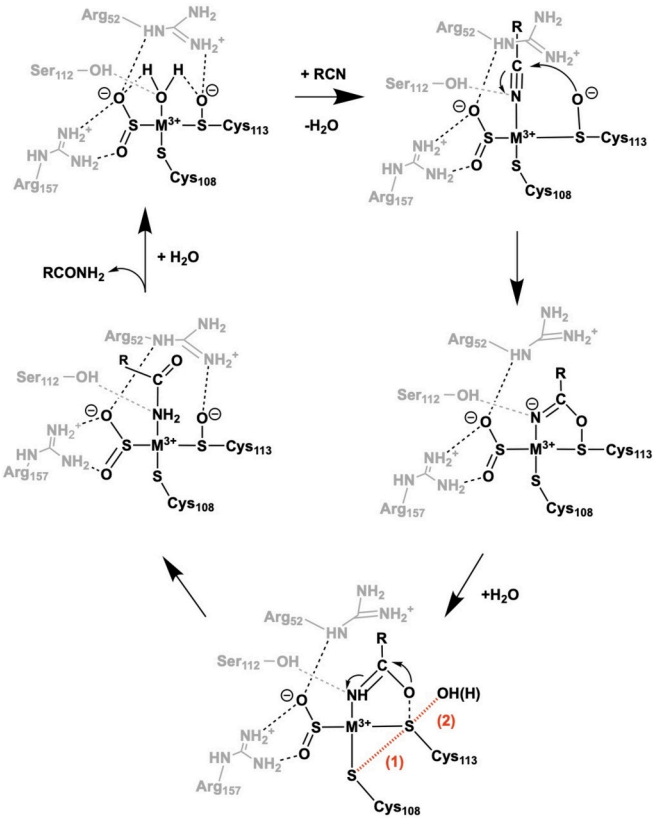

Fig. 6. Proposed mechanism of NHase catalysis, consistent with previous publications, with the conserved serine residue included. Red hashed lines indicate potential stabilizing disulfide bond (1) or the stabilization of the sulfur through the reformation of the sulfenic acid with a water molecule (2). Ligand numbering refers to *Pt*NHase system. (For interpretation of the references to color in this figure legend, the reader is referred to the web version of this article.)

reformation of the nucleophilic sulfenic acid. Therefore, the αSer residue appears to play an important role in catalysis as its presence markedly increases the rate of nitrile hydration, but its presence is not essential for catalysis. This work also confirms the necessity of the conserved second-sphere αSer residue for the metalation process and post-translational modification of the α-subunit for Co-type NHases but not Fe-type NHases, suggesting different mechanisms for the two types of NHases.

Funding

This work was supported by the National Science Foundation (CHE-2204024, RCH; and CHE-224023, BB and AF).

CRediT authorship contribution statement

Callie Miller: Writing – original draft, Visualization, Validation, Methodology, Investigation, Formal analysis, Data curation. **Kylie Knutson:** Writing – original draft, Investigation, Data curation. **Dali Liu:** Writing – review & editing, Visualization, Validation, Supervision. **Brian Bennett:** Writing – review & editing, Visualization, Validation, Supervision, Resources, Methodology, Investigation, Funding acquisition, Formal analysis, Data curation, Conceptualization. **Richard C. Holz:** Writing – review & editing, Supervision, Resources, Project administration, Methodology, Investigation, Funding acquisition, Formal analysis, Conceptualization.

Declaration of competing interest

The authors declare that they have no known competing financial interests or personal relationships that could have appeared to influence the work reported in this paper.

Data availability

Data will be made available on request.

References

[1] J.L. Legras, G. Chuzel, A. Arnaud, P. Galzy, Natural nitriles and their metabolism, World J. Microbiol. Biotechnol. 6 (1990) 83–108, https://doi.org/10.1007/BF01200927.

[2] H.S. Toogood, D. Mansell, J.M. Gardiner, N.S. Scrutton, 7.11 Reduction: enantioselective bioreduction of C–C double bonds, in: Comprehensive Chirality, Elsevier, 2012, pp. 216–255, https://doi.org/10.1016/B978-0-08-095167-6.00713-8.

[3] M. Boter, I. Diaz, Cyanogenesis, a plant defence strategy against herbivores, Int. J. Mol. Sci. 24 (2023) 6982, https://doi.org/10.3390/ijms24086982.

[4] C. Ramakrishna, H. Dave, M. Ravindranathan, Microbial metabolism of nitriles and its biotechnological potential, J. Sci. Ind. Res. 58 (1999) 925–947.

[5] R. Zheng, Y. Zheng, Y. Shen, Acrylamide, microbial production by nitrile hydratase, in: Encyclopedia of Industrial Biotechnology, Wiley, 2010, pp. 1–39, https://doi.org/10.1002/9780470054581.eib004.

[6] S. Arseniyadis, K.S. Kyler, D.S. Watt, Addition and substitution reactions of nitrile-stabilized carbanions, in: Organic Reactions, Wiley, 1984, pp. 1–364, https://doi.org/10.1002/0471264180.or031.01.

[7] V. Mylerova, L. Martinkova, Synthetic applications of nitrile-converting enzymes, Curr. Org. Chem. 7 (2003) 1–17, https://doi.org/10.2174/1385272033486486.

[8] S. Prasad, T.C. Bhalla, Nitrile hydratases (NHases): at the interface of academia and industry, Biotechnol. Adv. 28 (2010) 725–741, https://doi.org/10.1016/j.biotechadv.2010.05.020.

[9] H. Yamada, M. Kobayashi, Nitrile hydratase and its application to industrial production of acrylamide, Biosci. Biotechnol. Biochem. 60 (1996) 1391–1400, https://doi.org/10.1271/bbb.60.1391.

[10] J.K. Peter, R. Singh, A.K. Yadav, R. Kothari, P.K. Mehta, Toxicity of nitriles/amides-based products in the environment and their enzymatic bioremediation, J. Hazard. Mater. Adv. 13 (2024) 100389, https://doi.org/10.1016/j.hazadv.2023.100389.

[11] J. Baxter, S.P. Cummings, The current and future applications of microorganism in the bioremediation of cyanide contamination, Antonie Van Leeuwenhoek 90 (2006) 1–17, https://doi.org/10.1007/s10482-006-9057-y.

[12] A. Miyanaga, S. Fushinobu, K. Ito, T. Wakagi, Crystal structure of cobalt-containing nitrile hydratase, Biochem. Biophys. Res. Commun. (2001), https://doi.org/10.1006/bbrc.2001.5897.

[13] S. Martinez, R. Wu, R. Sanishvili, D. Liu, R. Holz, The active site sulfenic acid ligand in nitrile hydratases can function as a nucleophile, J. Am. Chem. Soc. (2014), https://doi.org/10.1021/ja410462j.

[14] Y. Yamanaka, Y. Kato, K. Hashimoto, K. Iida, K. Nagasawa, H. Nakayama, N. Dohmae, K. Noguchi, T. Noguchi, M. Yohda, M. Odaka, Time-resolved crystallography of the reaction intermediate of nitrile hydratase: revealing a role for the cysteinesulfenic acid ligand as a catalytic nucleophile, Angew. Chem. Int. Ed. (2015), https://doi.org/10.1002/anie.201502731.

[15] M. Nojiri, M. Yohda, M. Odaka, Y. Matsushita, M. Tsujimura, T. Yoshida, N. Dohmae, K. Takio, I. Endo, Functional expression of nitrile hydratase in Escherichia coli: requirement of a nitrile hydratase activator and post-translational modification of a ligand cysteine, J. Biochem. (1999), https://doi.org/10.1093/oxfordjournals.jbchem.a022339.

[16] Y. Yamanaka, K. Hashimoto, A. Ohtaki, K. Noguchi, M. Yohda, M. Odaka, Kinetic and structural studies on roles of the serine ligand and a strictly conserved tyrosine residue in nitrile hydratase, JBIC J. Biol. Inorg. Chem. 15 (2010) 655–665, https://doi.org/10.1007/s00775-010-0632-3.

[17] J. Lu, Y. Zheng, H. Yamagishi, M. Odaka, M. Tsujimura, M. Maeda, I. Endo, Motif CXCC in nitrile hydratase activator is critical for NHase biogenesis in vivo, FEBS Lett. (2003), https://doi.org/10.1016/S0014-5793(03)01070-6.

[18] Z. Zhou, Y. Hashimoto, K. Shiraki, M. Kobayashi, Discovery of posttranslational maturation by self-subunit swapping, Proc. Natl. Acad. Sci. USA (2008), https://doi.org/10.1073/pnas.0803428105.

[19] N. Gumataotao, K.P.W. Lankathilaka, B. Bennett, R.C. Holz, The iron-type nitrile hydratase activator protein is a GTPase, Biochem. J. (2017), https://doi.org/10.1042/BCJ20160884.

[20] Y. Xia, Z. Cheng, C. Hou, L. Peplowski, Z. Zhou, X. Chen, Discovery of the ATPase activity of a cobalt-type nitrile hydratase activator and its promoting effect on enzyme maturation, Biochem. Article AS (2022), https://doi.org/10.1021/acs.biochem.2c00167.

[21] Z. Zhou, Y. Hashimoto, M. Kobayashi, Self-subunit swapping chaperone needed for the maturation of multimeric metalloenzyme nitrile hydratase by a subunit exchange mechanism also carries out the oxidation of the metal ligand cysteine residues and insertion of cobalt, J. Biol. Chem. (2009), https://doi.org/10.1074/jbc.M808464200.

[22] Z. Zhou, Y. Hashimoto, T. Cui, Y. Washizawa, H. Mino, M. Kobayashi, Unique biogenesis of high-molecular mass multimeric metalloenzyme nitrile hydratase: intermediates and a proposed mechanism for self-subunit swapping maturation, Biochemistry (2010), https://doi.org/10.1021/bi100651v.

[23] C. Miller, D. Huntoon, N. Kaley, I. Ogutu, A. Fiedler, B. Bennett, D. Liu, R. Holz, Role of second-sphere arginine residues in metal binding and Metallocentre assembly in nitrile hydratases, J. Inorg. Biochem. 256 (2024) 112565, https://doi.org/10.1016/j.jinorgbio.2024.112565.

[24] K.P.W. Lankathilaka, B. Bennett, R.C. Holz, The Fe-type nitrile hydratase from *Rhodococcus equi* TG328-2 forms an alpha-activator protein complex, J. Biol. Inorg. Chem. (2020), https://doi.org/10.1007/s00775-020-01806-y.

[25] I.R.A.M. Ogutu, R.C. Holz, B. Bennett, Insight into the maturation process of the nitrile hydratase active site, Inorg. Chem. (2021), https://doi.org/10.1021/acs.inorgchem.0c02924.

[26] N. Gumataotao, M.L. Kuhn, N. Hajnas, R.C. Holz, Identification of an active site-bound nitrile hydratase intermediate through single turnover stopped-flow spectroscopy, J. Biol. Chem. (2013), https://doi.org/10.1074/jbc.M112.398909.

[27] I.R.A.M. Ogutu, M.St. Maurice, B. Bennett, R.C. Holz, Examination of the catalytic role of the axial cystine ligand in the co-type nitrile hydratase from pseudonocardia thermophila JCM 3095, Catalysts (2021), https://doi.org/10.3390/catal11111381.

[28] Y. Xia, L. Peplowski, Z. Cheng, T. Wang, Z. Liu, W. Cui, M. Kobayashi, Z. Zhou, Metallochaperone function of the self-subunit swapping chaperone involved in the maturation of subunit-fused cobalt-type nitrile hydratase, Biotechnol. Bioeng. (2019), https://doi.org/10.1002/bit.26865.

[29] S. Stoll, A. Schweiger, EasySpin, a comprehensive software package for spectral simulation and analysis in EPR, J. Magn. Reson. (2006), https://doi.org/10.1016/j.jmr.2005.08.013.

[30] W. Kabsch, XDS, Acta Crystallogr. D Biol. Crystallogr. 66 (2010) 125–132, https://doi.org/10.1107/S0907444909047337.

[31] D. Liebschner, P.V. Afonine, M.L. Baker, G. Bunkóczi, V.B. Chen, T.I. Croll, B. Hintze, L.-W. Hung, S. Jain, A.J. McCoy, N.W. Moriarty, R.D. Oeffner, B.K. Poon, M.G. Prisant, R.J. Read, J.S. Richardson, D.C. Richardson, M.D. Sammito, O. V. Sobolev, D.H. Stockwell, T.C. Terwilliger, A.G. Urzhumtsev, L.L. Videau, C. J. Williams, P.D. Adams, Macromolecular structure determination using X-rays, neutrons and electrons: recent developments in *Phenix*, Acta Crystallogr. D Struct. Biol. 75 (2019) 861–877, https://doi.org/10.1107/S2059798319011471.

[32] L.L.C. Schrödinger, The PyMOL Molecular Graphics System, Version~1.8, 2015.

[33] J. Shearer, H.L. Jackson, D. Schweitzer, D.K. Rittenberg, T.M. Leavy, W. Kaminsky, R.C. Scarrow, J.A. Kovacs, The first example of a nitrile hydratase model complex that reversibly binds nitriles, J. Am. Chem. Soc. 124 (2002) 11417–11428, https://doi.org/10.1021/ja012555f.

[34] S. Martinez, X. Yang, B. Bennett, R.C. Holz, A cobalt-containing eukaryotic nitrile hydratase, Biochim. Biophys. Acta, Proteins Proteomics (2017), https://doi.org/10.1016/j.bbapap.2016.09.013.

[35] J. Shearer, I.Y. Kung, S. Lovell, W. Kaminsky, J.A. Kovacs, Why is there an “inert” metal center in the active site of nitrile hydratase? Reactivity and ligand dissociation from a five-coordinate co(III) nitrile hydratase model, J. Am. Chem. Soc. 123 (2001) 463–468, https://doi.org/10.1021/ja002642s.

[36] K.P.W. Lankathilaka, N. Stein, R.C. Holz, B. Bennett, Cellular maturation of an iron-type nitrile hydratase interrogated using EPR spectroscopy, JBIC J. Biol. Inorg. Chem. 24 (2019) 1105–1113, https://doi.org/10.1007/s00775-019-01720-y.

[37] A. Miyanaga, S. Fushinobu, K. Ito, H. Shoun, T. Wakagi, Mutational and structural analysis of cobalt-containing nitrile hydratase on substrate and metal binding, Eur. J. Biochem. (2004), https://doi.org/10.1046/j.1432-1033.2003.03943.x.

[38] M. Prejanò, T. Marino, C. Rizzuto, J.C. Madrid Madrid, N. Russo, M. Toscano, Reaction mechanism of low-spin Iron(III)- and cobalt(III)-containing nitrile hydratases: a quantum mechanics investigation, Inorg. Chem. (2017), https://doi.org/10.1021/acs.inorgchem.7b02121.

[39] T.K. Harris, A.S. Mildvan, High-precision measurement of hydrogen bond lengths in proteins by nuclear magnetic resonance methods, proteins: structure, Funct. Genet. 35 (1999), https://doi.org/10.1002/(SICI)1097-0134(19990515)35:3<275::AID-PROT1>3.0.CO;2-V.

[40] K. Hashimoto, H. Suzuki, K. Taniguchi, T. Noguchi, M. Yohda, M. Odaka, Catalytic mechanism of nitrile hydratase proposed by time-resolved X-ray crystallography using a novel substrate, tert-butylisonitrile, J. Biol. Chem. (2008), https://doi.org/10.1074/jbc.M806577200.

[41] S. Mitra, R.C. Holz, Unraveling the catalytic mechanism of nitrile hydratases, J. Biol. Chem. (2007), https://doi.org/10.1074/jbc.M604117200.

[42] W.L. Karunagala Pathiranage, N. Gumataotao, A.T. Fiedler, R.C. Holz, B. Bennett, Identification of an intermediate species along the nitrile hydratase reaction pathway by EPR spectroscopy, Biochemistry (2021), https://doi.org/10.1021/acs.biochem.1c00574.